RSC Advances

RSC Publishing

PAPER

View Article Online
View Journal | View Issue

Cite this: *RSC Advances*, 2013, **3**, 11571

Determination of the energy landscape of $Pd_{12}Pt_1$ using a combined genetic algorithm and threshold energy method†

Rafael Pacheco-Contreras,[a] Dora J. Borbón-González,[b] Maribel Dessens-Félix,[c] Lauro Oliver Paz-Borbón,[d] Roy L. Johnston,*[e] J. Christian Schön,*[f] Martin Jansen[f] and Alvaro Posada-Amarillas*[a]

Received 17th December 2012,
Accepted 17th April 2013

DOI: 10.1039/c3ra41477a

www.rsc.org/advances

In this work we present a thorough exploration of the potential energy surface (PES) of Pd–Pt bimetallic nanoparticles at the specific composition $Pd_{12}Pt_1$, using the combination of a genetic algorithm and the threshold method for global optimization and exploration of the barrier structure, employing the semi-empirical Gupta many-body potential for modeling the interatomic interactions. The structural and energetic analysis of $Pd_{12}Pt_1$ nanoparticles, including binding energies (E_b), symmetries and common-neighbor analysis (CNA) allowed us to identify a large set of representative structures of local minima, with an icosahedral motif found to be the putative global minimum for $Pd_{12}Pt_1$. A detailed study of the icosahedral motif was carried out by an exhaustive exploration of low energy isomers, in order to understand qualitatively structural interconversion. 2-D tree (disconnectivity) graphs are plotted to map the structures of minima on the PES of $Pd_{12}Pt_1$. DFT calculations were performed on representative structures to establish the energetic hierarchy and structural stability.

1. Introduction

In recent years there has been a tremendous growth in interest in bimetallic and multi-metallic clusters (also known as ''nanoalloys''),[1] because of their applications in strategic value-adding industries, these being principally the petrochemical, pharmaceutical and clean-energy sectors.[2–7] At the nanoscale, metallic nanoalloys have a high surface/volume ratio implying a large number of surface atoms, a vital property which makes them ideal as catalysts, as many reactions take place at nanoparticle surface sites. Nanoalloys thus represent a new type of material often displaying unique characteristics which differ from their corresponding constituent atoms or bulk matter.[4–10]

Compared to monometallic clusters, bimetallic nanoalloys such as Pd–Pt show a wider range of structural possibilities. It is known that the preparation conditions of the bimetallic nanoparticles can directly influence their size, shape and segregation properties.[5,11] Using a combination of experimental techniques (transmission electron microscopy (TEM), x-ray absorption spectroscopy (XAS) and low energy ion scattering (LEIS)), Renouprez, Rousset *et al.* demonstrated that their Pd–Pt nanoparticles (with diameters of 1–5 nm) were truncated octahedra with a Pt-rich core surrounded by a Pd-rich shell.[8,9] Bazin *et al.* have studied supported Pd–Pt nanoalloys deposited on γ-alumina, using a combination of XAS, TEM and volumetric H_2O_2 titration. They showed that their Pd–Pt particles, with sizes <1 nm, had ''cherry-like'' (spherical) structures with Pt atoms occupying core sites and with Pd atoms decorating the surface.[10] Habas *et al.* have also reported the characterization of $Pt_{core}Pd_{shell}$ nanoparticles, obtained by epitaxial seeded growth.[12] On the other hand, D'Souza and Sampath have reported the preparation of Pd–Pt nanoparticles by the sol–gel process. These bimetallic nanoparticles (with sizes 1–3 nm) were characterized by X-ray photoelectron spectroscopy (XPS) and CO adsorption measurements, the results of which indicated that the particles have a Pd core and a Pt shell.[13] Sanchez *et al.* have shown, using high angle annular dark field scanning transmission electron microscopy (HAADF-STEM), that $Pt_{core}Pd_{shell}$, $Pd_{core}Pt_{shell}$ or alloyed Pd–Pt

[a]*Departamento de Investigación en Física, Universidad de Sonora, Apdo. Postal 5-088, 83190 Hermosillo, Sonora, México. E-mail: posada@cajeme.cifus.uson.mx*
[b]*Departamento de Matemáticas, Universidad de Sonora, 83000 Hermosillo, Sonora, México*
[c]*Programa de Doctorado en Ciencias de Materiales, Universidad de Sonora, 83000 Hermosillo, Sonora, México*
[d]*Department of Applied Physics and Competence Centre for Catalysis, Chalmers University of Technology, SE-41296 Göteborg, Sweden*
[e]*School of Chemistry, University of Birmingham, Edgbaston, B15 2TT, Birmingham, UK. E-mail: r.l.johnston@bham.ac.uk*
[f]*Max-Planck Institute for Solid State Research, Heisenbergstrasse 1, D-70569 Stuttgart, Germany. E-mail: C.Schoen@fkf.mpg.de*
† Electronic supplementary information (ESI) available. See DOI: 10.1039/c3ra41477a

configurations can be generated by sequential reduction or co-reduction of Pd and Pt salts.[14]

From a theoretical point of view, a challenging problem in cluster science is to determine the most stable isomer of a particular cluster for a given size (number of atoms) and composition as this involves optimizing both the geometry and chemical ordering (degree of segregation or mixing). It is currently accepted that finding the structural ground state of clusters is a difficult task, even if we deal with an homogeneous metal nanoparticle, and exhaustive potential energy surface (PES) searches are essential in order to have a reasonable probability of finding the global minimum (GM), due to the exponential increase in geometrical isomers with the number of atoms.[15–17] For the case of bimetallic (binary) nanoparticles, the problem increases dramatically, as for each geometrical isomer there is a combinatorial dependence of the number of homotops (inequivalent permutational isomers) on the composition.[18] Global optimization techniques,[19–23] such as genetic algorithms,[24–27] basin hopping Monte Carlo[28–30] and the threshold method[31,32] have been developed to overcome this problem. This has allowed the exploration of large regions of the PES of monometallic and bimetallic nanoparticles (both in the gas-phase or supported on an oxide substrate) and the successful identification of their corresponding GM structures within a vast number of geometrical isomers and homotops.

Since the pioneering work of Goldstein,[33] it has been clear that many of the intrinsic physical and chemical properties of complex systems (*e.g.* crystalline solids, nanoclusters, and biological systems such as proteins) are directly determined by their corresponding PES.[20,21,33–35] An accurate PES description is thus needed in order to locate the putative GM configuration as well as the pathways connecting them *via* the corresponding transition states (TS) to other local-minimum configurations.

In this work we present a thorough exploration of the PES for the bimetallic cluster $Pd_{12}Pt_1$, using a combination of a genetic algorithm and the threshold method for global optimization and exploration of the barrier structure, employing the semi-empirical Gupta many-body potential for modeling the interatomic interactions. Structural and energetic analysis of $Pd_{12}Pt_1$ nanoparticles include the calculation of binding energies (E_b), common-neighbor analysis (CNA) indices and their normalized relative abundance (RA)[36] in order to understand plausible structural interconversion. It is worth mentioning that the CNA technique gives a three-dimensional representation of the atomic configuration around a selected bonded pair of atoms (root pair) which facilitate the structural classification in terms of a set of three numbers (indices) that provide the order type and corresponding abundance.[37] Tree graphs[32,38–41] are plotted to map both the representative structures of the minima on the PES of $Pd_{12}Pt_1$ and a variety of archetypical multiply twinned (MT) structures found in our searches. Prominent structural isomers were found in our searches, ranging for example, from helical (right and left-handed) configurations and slightly distorted biplanar (BP) structures to icosahedral motifs (Ih). The minimum energy configuration in the case of the BP structure has the Pt atom located at the center of the hexagonal plane, while in the helical structures the minimum energy configuration has the Pt atom in the second position of the 5-atom strand. Disconnectivity graphs show the homotops energetical ordering of selected MT structures, rationalizing the different tetrahedral growth types in terms of some basic information provided by the energy landscape analysis. Energy landscape analysis including the determination of the barrier structure is a novel approach for bimetallic clusters, and has been utilized to generate a representation of a partial PES region,[61] thus yielding a deeper understanding of the entire potential energy surface.

Finally, the relative stability of putative minima is tested against more accurate methods, namely density functional theory (DFT).[42,43] Full relaxations are carried out on selected configurations and the results are discussed in terms of the energetic ordering and structural properties of these clusters, including the novel helical and biplanar $Pd_{12}Pt_1$ nanoparticles.

2. Methodology

2.1 The Gupta potential

In this study, the intermetallic interaction is modeled by the Gupta many-body potential,[44] which is a phenomenological potential energy function that has been shown to describe transition and noble metal cluster structures reasonably accurately.[45] The Gupta potential is an example of a many-body potential which is based on the second-moment approximation of the tight binding density of states. The potential consists of a two-body repulsive component and a many-body attractive component. The homonuclear parameters are fitted to the cohesive energy, lattice parameter and independent elastic constants for the bulk metals in the corresponding crystal structure at 0 K. The heteronuclear (Pd–Pt) parameters used here are the average parameters introduced by Massen *et al.*[46] which have been used previously.[26] At the Gupta potential level of theory, the binding energy (E_b) per atom of a cluster in our work is calculated as the total energy of the cluster (E_{Total}), divided by the total number of atoms (N). Thus, negative values imply improved structural stability.

2.2 Parameters of the *ab initio* DFT calculations

DFT calculations are performed on selected minima structures using Dmol3 software.[47–49] A gradient corrected exchange–correlation functional is employed as proposed by Perdew, Burke and Ernzerhof (PBE).[50] The one-electron Kohn–Sham orbitals are expanded in a localized numerical basis set. A double numerical basis set is used together with polarization functions (dnp). A real space cutoff of 4.9 Å is used for the basis functions. A pseudo potential[51] which also accounts for the relativistic effects is employed for Pd and Pt to describe the interaction between the valence electrons and the nuclei together with the inner shell electrons. The states treated in the valence shell are $4s^2 4p^6 4d^{10}$ and $5s^2 5p^6 5d^9 6s^1$ for Pd and Pt, respectively. The Kohn–Sham equations are solved self-

consistently using an integration technique based on weighted overlapping spheres centered at each atom. The direct Coulomb potential is obtained by projection of the charge density onto angular dependent weighting functions also centered at each atom. The Poisson equation is, thereafter, solved by one-dimensional integration. Cluster geometry optimizations are performed without imposing symmetry constraints by the use of the BFGS method.[52–55] Structures are considered to be relaxed when changes in the energy, the largest element of the gradient and the atomic displacements are smaller than 10^{-5} Ha (*i.e.* 2.72×10^{-4} eV), 0.05 eV Å^{-1} and 0.005 Å, respectively. All calculations are performed spin unrestricted. The relative stability of the different $Pd_{12}Pt_1$ cluster geometries is analyzed at the DFT level by calculating their corresponding average binding energy per atom:

$$E_b = [E(Pt_{12}Pt_1) - 12 \cdot E(Pd_{atom}) - 1 \cdot E(Pt_{atom})]/N \quad (1)$$

where N denotes the total number of atoms in the bimetallic cluster.

2.3 The genetic algorithm

Genetic algorithms (GA) are global search optimization techniques, based on the concepts of natural selection, which have been widely used to obtain minimum energy structures of atomic and molecular clusters.[56] Initially, a collection of individuals (clusters) is generated at random and then energy-minimized to produce an initial population, where each member of the population corresponds to a local minimum on the PES. Secondly, a fitness function is used by the GA in order to determine which individuals will survive from one generation to the next. The fitness value depends on the cluster's total energy such that low-energy clusters will have high fitness and *vice versa*. Subsequently, individuals are selected to take part in crossover (''mating'') based on their fitness. A cluster is accepted for mating if its fitness value is greater than a randomly generated number between 0 and 1. In this way, parent structures are combined in order to generate offspring. Crossover moves are performed using the "cut-and-splice" method introduced by Deaven and Ho,[57] which involves randomly rotating two parent clusters, cutting both horizontally in one or two positions and then combining complementary fragments.[58] As in nature, mutation is introduced in order to maintain population diversity. In our optimizations, each cluster has the same probability of being mutated.[58] The specific details of the GA we have adopted[56] and the descriptions of previous applications can be found elsewhere.[26,46,59]

2.3 The threshold energy method

2.3.1 Description of method. In order to survey the PES of $Pd_{12}Pt_1$, we have used the threshold method.[31,32] This is a Monte Carlo based approach which makes use of random walks below a sequence of prescribed energy lids combined with stochastic quenches. This method requires a low-energy configuration usually obtained from other optimization techniques (in this case the GA) initial input. Starting from the GM or a local minimum, random walks are carried out through the configurational space, under the constraint that a given energy E_{lid} threshold is not exceeded all moves that fulfill this criterion are accepted. After a certain number of steps the system is relaxed into one neighboring minimum. One usually performs several stochastic quenches from the same stopping point in order to determine whether the walker is inside a basin or in a transition region. By carrying out a number of Monte Carlo runs at different E_{lid} values, energy barriers separating the putative GM from other (higher-energy) minimum structures can be estimated. Such a set of threshold runs is repeated starting from many local minima on the landscape. In this way, the iterative procedure allows us to carefully explore the PES landscape.

A set of simulation parameters selected to facilitate an extensive exploration of the PES determine the success of finding minimum energy structures. Their values depend on the system's size, the number of chemical elements involved, the PES function complexity, *etc.* In this study, the parameters needed in the G42‡ code were obtained as a result of running several tests before finding the simulation conditions which allowed us to have the most accurate view of the PES belonging to the $Pd_{12}Pt_1$ nanoalloy.

2.3.2 Application to the specific system under investigation. Particular details of the PES exploration are as follows: a ladder of 30 energy lids (E_{lid}) was constructed in order to carry out each of the runs; the energy gap between successive lids was 0.1 eV/atom. The first lid was placed at −3.5 eV/atom, an energy value slightly above that corresponding to the icosahedral structure, whereas the final lid was placed very close to the cluster's dissociation energy, at −0.6 eV/atom. Within this energy window, the system was allowed to evolve in order to access several local minima. For each run below every energy lid, a different seed was used, releasing a set of random walkers for each seed. The random walks in each run accept movements limited by the value of the energy lid, a procedure which will eventually give access to other local minima by crossing energy barriers. Three different seeds were used for each energy lid, 10 random walkers for each seed giving each walker 2.5×10^5 Monte Carlo steps and, at the stopping point, 20 stochastic quenches of 2.5×10^5 steps each, to find out if the random walk had led to another local minimum. Local relaxations were carried out on each new structure in order to reach the bottom of the local basin. The L-BFGS-B algorithm of Zhu *et al.*[60] was used at the end of each quench to efficiently reach the bottom of the basin.

The threshold runs provided 18 000 configuration files which were analyzed taking into account structural and energetic criteria (CNA indices and total energy). We found only 5016 different configurations (minima) which permit us, at least in principle, to gain insight on the $Pd_{12}Pt_1$ cluster PES, *i.e.*, on the physical and chemical properties of this nanoalloy. It was necessary to analyze the morphology of each of the different configurations to elucidate the existence of structural or compositional variations. This procedure yielded 79 structures and made it possible to build the disconnectivity graph for the energy region where these structures were found computationally. For this, 25 structures out of the 79 were

‡ G42 is a modular code consisting of a large package of routines for the exploration of energy landscapes.

chosen as representatives of the cluster's energy landscape, based on geometrical and compositional considerations.

After identifying the different structures with the lowest local energy, we constructed their disconnectivity graphs starting in the lowest energy minimum selected for each isomer and employing a set of 10 energy thresholds with a spacing between energy lids of 0.01 eV/atom. Reaching the top energy lid allows us to determine the corresponding energy barrier for each of the isomers found in the global exploration. Considering the stochastic nature of the TM and the fact that the number of steps performed by the walkers is finite, there is always a possibility that some minima cannot be reached even if there exists a trajectory under some energy lid. However, the occurrence of a structural transition from a given structure to another can be explored systematically by means of an appropriate procedure.

In order to extract further information about the equilibrium properties of the isomers with the lowest energy values, additional threshold runs were carried out by defining a particular energy exploration region for selected structures. These target structures were chosen mainly because we expected to find sets of homotops (*e.g.* the tetrahelices), or due to their apparent polytetrahedral (isotropic or anisotropic) growth behavior. Ten energy lids were generated, starting from the corresponding local minimum, giving a spacing of 0.01 eV/atom between energy lids. This procedure allowed us to distinguish the corresponding energy barriers between different local minima distributed throughout the hypersurface, obtained from the G42 runs. In this way, several new local minimum configurations of $Pd_{12}Pt_1$ clusters were located, and used as starting configurations in new explorative PES searches (with identical computer simulation conditions), performed to obtain a deeper understanding around the selected local minima structures. This methodology permitted us previously to identify a set of enantiomeric helical structures,[61] detected in an energy region where axial growth of fused tetrahedra (sharing faces or edges) are local minima. In the present work, we extend the analysis choosing a set of computational parameters appropriate for a global PES exploration.

3. Results and discussion

Table 1 (in the ESI†) lists 25 representatives of the structurally diverse minima found after performing an exhaustive exploration of the $Pd_{12}Pt_1$ cluster PES. The putative GM corresponds to an icosahedral structure, in which the Pt atom occupies the core position (Ih). The CNA indices and their normalized RA provide an indication of the type and degree of order as the energy increases. Several types of pairs characterize different types of order,[62] for instance, an icosahedral packing arrangement is defined by indices 555, whereas 421 and 422 are typical of fcc and hcp order. In our results, the lowest energy icosahedral structure exhibits only 555 (~29%) and 322 (~71%) indices. This structure is an example of isotropic tetrahedral growth, obtained by joining tetrahedra with no preferred stacking. The existence of non-equilateral triangular faces, defined by 322 indices, may be associated with the tetrahedral coordination of this structure while 555 indices define the presence of pentagonal planes as characteristic geometrical elements of this structure.

Relevant higher energy structures are: a fragment of a waist-capped Ino truncated decahedron (Ih-Ino); a fcc BP structure with a small distortion due to the presence of the Pt atom, which was confirmed through local reoptimizations of all the homotops after changing the Pt atom to Pd; linear stacking of tetrahedra forming chiral pairs of right-handed and left-handed helices (HR and HL); fragments of a double icosahedron (MT-Ih2 and MT-Ih3); a structure composed of two edge-connected pentagonal bipyramids, sharing a capped atom over this edge (S6); a polytetrahedral elongated cluster exhibiting two coupled square bipyramids, resembling a monoclinic structure (S13) and some other structures showing both isotropic and anisotropic polytetrahedral growth. The latter are elongated structures appearing in high energy regions, usually for energy values above −3.365 eV/atom. These elongated structures are formed by multiple, twisted or straight strands of atoms. Amorphous structures were also found in our search, as well as a large number of other distorted icosahedral, decahedral and biplanar structures. These have been omitted as they only constituted ~1% of the minima found during our PES search. Fig. 1 displays the multiple funnel palm-tree type[16] energy landscape obtained from exploring the semi-empirical potential energy hypersurface.

Once an initial exhaustive global exploration of the $Pd_{12}Pt_1$ cluster PES had been carried out, we then focused on the lowest energy structure, *i.e.* the putative icosahedral GM structure (see Table 1,† Ih), and used this configuration as the initial structure for additional threshold method runs. Fig. 2 shows the different icosahedron-related local-minima found after carrying out the new PES exploration. Four different icosahedron-based configurations were located, and

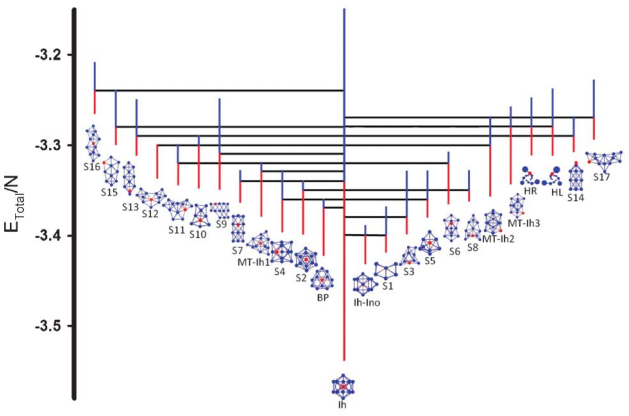

Fig. 1 Tree (disconnectivity) graph showing the most abundant structures on the $Pd_{12}Pt_1$ potential energy hypersurface. The black horizontal lines indicate energy lid positions; the vertical red lines give the magnitudes of the energy barriers, while the blue vertical lines indicate the last energy lid where this structure was found.

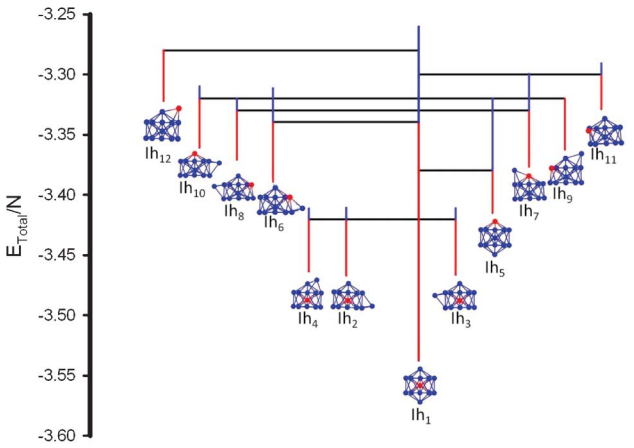

Fig. 2 Tree (disconnectivity) graph indicating the possible interconversion pathways between icosahedral-like structures. Structural interconversion between homotops is in the energy range explored by the random walk. The color code is the same as in Fig. 1.

several homotops were also identified, giving a total of 12 structures. These structures can be described starting with the lowest energy structure as follows: icosahedron (Ih_1); truncated icosahedron with one waist-down capping Pd atom (Ih_2); truncated icosahedron with one waist-up capping Pd atom (Ih_3); truncated icosahedron with one top face-capping Pd atom (Ih_4) (it should be noted that structures Ih_1 to Ih_4 all have the Pt atom in the central site of the parent icosahedron); homotop of Ih_1 with the Pt atom in the shell; homotop of Ih_2 with Pt at the apex (Ih_6); homotops of Ih_3 with Pt in a pentagonal plane (Ih_8), at the top (Ih_{10}) and in the waist-up capping position (Ih_{11}); 3 homotops of Ih_4 with Pt at the top (Ih_7), in the upper pentagonal plane (Ih_9), and as a capping atom (I_{12}). Despite the vast PES analysis carried out by our global optimization strategies, we are aware that many other possible homotops were not reached by our search methods. Consider, for example, the right-handed helical structures where all the 7 homotops (considering symmetry) are found just by changing the Pt atom position. The obtained configurations are grouped together in Table 2 (ESI†) for clarity, where we give additional structural and energetic details.

Our results show that the energy of low-lying structures varies with the number of Pt–Pd bonds, energetically favoring those structures that have a higher number of Pt–Pd bonds (see Table 2†). The effect of the varying number of Pt–Pd bonds can be seen by comparing the structures of the homotops Ih_1 and Ih_{12}. In Ih_1 we found the maximum number of Pt–Pd bonds (12). On the other hand, Ih_{12} has only 3 Pt–Pd bonds. A similar relationship holds for homotops Ih_3, Ih_8, Ih_{10} and Ih_{11}, where the number of Pt–Pd bonds is 11, Ih_3, Ih_8 and Ih_{10} have 6 and Ih_{11} has only 3. An analogous analysis can be performed for the homotops (Ih_2, Ih_6) and (Ih_4, Ih_7, Ih_9).

A tree or disconnectivity graph[32,38–41] was constructed to gain a better picture of the $Pd_{12}Pt_1$ complex hypersurface. In order to construct these diagrams, we grouped all those configurations having identical total energy and CNA indices, *i.e.* those with essentially the same structure up to permutational symmetry operations, into one basin (see Fig. 1). Fig. 2 shows the tree graph arising from the refined exploration centered on the GM icosahedral structure (Ih_1), thus giving a more precise representation of the unique energy landscape of the $Pd_{12}Pt_1$ cluster in terms of structures Ih_1 to Ih_{12} within the energy range −3.5 eV/atom to −3.3 eV/atom, which correspond to the lower region of the PES. In this figure, a single transition state connects local minima, but we note that potential structural interconversions, even in this simplistic representation, are affected by the physical nature of the barrier, energetic or entropic.

When the random walker performs a finite number of steps and moves a finite distance, there is a certain probability that the system will not reach a particular target minimum from a given starting minimum, even if a (short enough) pathway below the energy lid between the two neighboring minima exists. The reason for this is that in high-dimensional spaces the likelihood to find such a fast low-energy route between two minima is not only controlled by energetic barriers but also by entropic and/or kinetic barriers taking the width of the transition regions and the internal structure of the basins into account. All these aspects are subsumed under the concept of a generalized barrier discussed elsewhere[63] that can be quantified *via* the logarithm of the inverse transition probability obtained by counting the number of successful transitions between the minima under consideration. In Fig. 2 we show the 12 different $Pd_{12}Pt_1$ cluster structures (Ih_1–Ih_{12}), all of which correspond to local minima on the PES. Structural interconversion may be rationalized as a process that transforms one structure into another by crossing the energy barrier connecting the two minima, promoted by physical or chemical processes.

One particularly interesting feature is the grouping of minima on the landscape according to their underlying structure (*i.e.*, modulo the homotopy§). Both the barriers and the energy differences among the helical structures and also among the biplanar structures are quite low compared with the typical differences among structurally distinct isomers. While this is not too surprising as far as the energies are concerned, the rather small barriers, of about 0.05 eV/atom, are somewhat surprising, since the transformations involve complex atom exchange paths. However, the fact that most atoms can be considered surface atoms is a likely cause for such low-energy transition routes between members of a structural group. As a consequence, we would expect that homotopically related isomers can relatively easily transform into each other, at least in the case of small intermetallic clusters.

Our computational surface energy analysis allowed us to find other relevant structures discussed recently in the scientific literature,[61,64–73] some of which are important for

§ The homotopy group H is the set of all atom exchange operations that exchange atoms of different atom type.

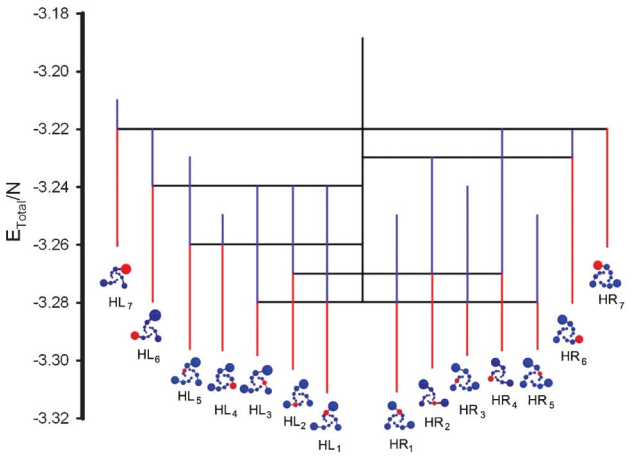

Fig. 3 Tree (disconnectivity) graph exhibiting the energy landscape region where helical enantiomeric structures are abundant. The color code is the same as in Fig. 1.

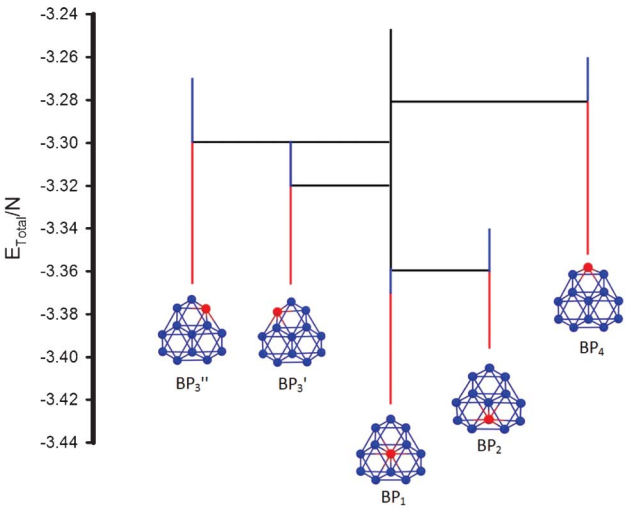

Fig. 4 Possible homotops BP_1–BP_4 (and enantiomers BP_3' and BP_3'') of the biplanar structure for the $Pd_{12}Pt_1$ cluster. The tree (disconnectivity) graph shows the structural distribution according to the energy of each configuration. The color code is the same as in Fig. 1.

current or potential practical technological applications. Besides biological examples, in diverse synthesis procedures based on chemical or physical methods, structures with helical symmetry appear as a result of experimental conditions and forces governing interactions between atoms. This motivated an investigation of the geometric structures of some of the elongated $Pd_{12}Pt_1$ clusters existing on the PES, which we published very recently,[61] describing a subset of enantiomeric helical structures ("Bernal spirals"[64–67]) resembling those found experimentally for Au–Ag nanowires.[68] Computational restriction means that we have been unable to carry out an exhaustive PES exploration, so several structures were not found during the search but have been subsequently generated (based on symmetry) and then locally minimized. Current results, shown in Fig. 3 as a tree graph, present a set of 14 multitwinned tetrahelices, 7 right-handed and 7 left-handed. The atomic distribution on strands and the helix symmetry for the $Pd_{12}Pt_1$ nanoalloy reduce the number of inequivalent homotops to 7; therefore our current searches provided all the expected right-handed structures and 6 out of 7 of the left-handed ones. The left-handed structure HL_5 was not reached even though the energy threshold between the lids used in this work had a value of 0.01 eV/atom, *i.e.*, half the spacing used previously.[61] Additional structural and energetical details are given in Table 3 (see the ESI†), where the missing left-handed structure was built by hand and locally optimized to provide complete information. Notice that the difference in the barrier heights of the left- and right-handed modifications is due to sampling effects, and the best estimate of the energy barrier is the lower of the two values.

The 13-atom transition and noble metal biplanar cluster is another important structure which has been repeatedly reported since it was theoretically discovered by Chang and Chou[69] by means of structural optimizations based on first principle DFT calculations.[70–73] These BP (distorted) structures have been reported to be ground state structures in a number of pure metal clusters.[69–71,73] Most of these studies agree with the idea that 13-atom Pd and Pt clusters adopt the BP structure as the ground state configuration, nevertheless, to date there are only a few very recent studies reporting BP structures for bimetallic systems[72] by any of the current theoretical methods to search for the lowest energy structures, *i.e.*, using DFT or semi-empirical potentials. Even though the Gupta potential tends to give 3-D ground state structures, our global exploration allows us to have a better idea of the structural families belonging to a particular PES.

The results reported here also include those for BP $Pd_{12}Pt_1$ structures, which are not the lowest energy structures (see Fig. 1 and Table 4 in the ESI†) but correspond to local minima on the Gupta potential energy hypersurface. The parent Pd_{13} BP structure has C_{3v} symmetry and consists of a plane of 6 atoms forming a triangle and a plane of 7 atoms forming a centered hexagon. Upon substituting one Pd atom by Pt, 4 homotops can be generated for BP $Pd_{12}Pt_1$ (which we have named BP_1–BP_4, in order of increasing energy): the disconnectivity diagram for the BP isomers $Pd_{12}Pt_1$ is shown in Fig. 4. The homotops can be described as follows: BP_1—the Pt lies in the center of the hexagonal plane; BP_2—the Pt lies in the inner triangle of the triangular plane; BP_3—the Pt lies on the periphery of the hexagonal plane; BP_4—the Pt lies in the outer triangle of the triangular plane. Homotops BP_1, BP_2 and BP_4 are achiral (having C_s symmetry), as the Pt atom lies on a mirror plane of symmetry. However, as the Pt atom in homotop BP_3 does not lie on a mirror plane of the parent BP structure, this homotop is chiral, existing as the enantiomeric pair BP_3' and BP_3'' which confirms that chirality is recurrent in bimetallic clusters.[61,74]

Finally, we verified the structural stability and established the ranking of the $Pd_{12}Pt_1$ clusters by energy using more accurate first principles methods (see Section 2.2). For this, a

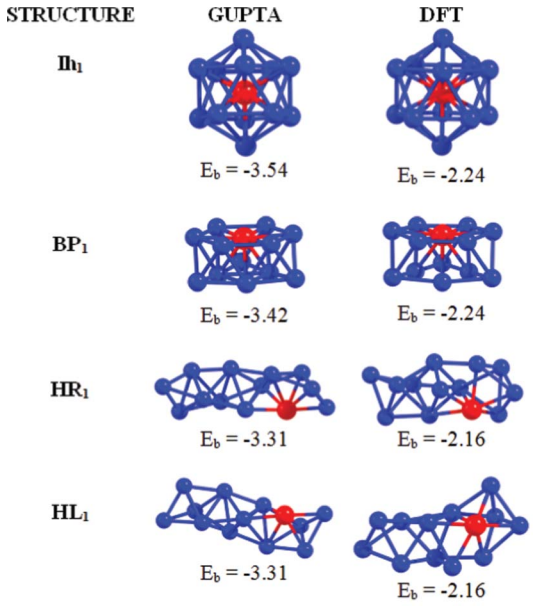

Fig. 5 Energetical ordering of selected lowest energy configurations, according to semiempirical (Gupta potential) and DFT calculations. The binding energy (E_b) is in eV/atom.

set of representative minimum energy structures, *i.e.* Ih_1, HR_1, HL_1 and BP_1 were selected for further DFT reoptimizations. As far as the authors are aware, no DFT calculations have been reported previously for these structures. After relaxation, we observed that all the optimized structures presented slightly longer Pd–Pd and Pd–Pt bonds (by approximately 0.13 Å), compared to the Gupta ones. However, such small changes are sufficient to distort the helical structure of the HL_1 and HR_1 clusters, as the Pt atom tries to maximize the number of interactions with neighboring Pd atoms. The $Pd_{12}Pt_1$ clusters are characterized by large magnetic moments: $HL_1/HR_1 = 4\ \mu_B$; $BP_1 = 6\ \mu_B$ and $Ih_1 = 8\ \mu_B$. Overall, the Ih_1 structure remained the lowest in energy; though it is only 0.1 eV lower in total energy than the planar BP_1 structure. This is because of the larger number of Pd–Pt bonds in the Ih_1 structure (12) compared to the BP1 structure (9). In terms of the binding energy, the Ih_1 and BP_1 structures have the same value to two decimal places: 2.24 eV. The helical HR_1 and HL_1 structures are found to be rather high in total energy (1.13 eV) compared to the Ih_1 cluster, with a calculated E_b value of 2.16 eV for both cases. The relaxed structures and energies are shown in Fig. 5.

Our results show that, even at the higher level of theory, the energetic ordering predicted by the semi-empirical potential and global optimization methods is preserved, and that the conclusions arising from our global searches remain valid. Similar energetic trends have recently been reported by Ferrando *et al.* for larger Pd–Pt clusters, comparing semi-empirical Gupta potential minima and DFT optimized configurations.[75] In their work, the putative Gupta minimum became a high-energy isomer at the DFT level; thus highlighting the need to test the reliability of the potential against electronic structure methods even though the computational cost can be rather high. It is important to emphasize that the results reported in ref. 75 correspond to searches for low-lying minima, rather than mapping the energy landscape or calculating the energy barriers to isomerization. Here, we describe a different, insightful process which provides a good description of the full potential energy surface and which allows us to realize *e.g.* that homotopically related structures are separated by comparatively low barriers. In addition, based on our DFT calculations, we predict that the lowest energy structures reported in this work for these bimetallic clusters can co-exist under appropriate experimental conditions (*e.g.* temperature, pressure and support type).[68]

4. Conclusions

In this work we have established the appropriateness of using combined optimization (genetic algorithm and the threshold method) schemes in order to explore the complex PES of a bimetallic $Pd_{12}Pt_1$ nanoalloy, as modeled by the Gupta many-body potential. A thorough analysis of the cluster PES allowed us to locate and identify a set of representative structures, where an icosahedral structure was unambiguously found as the corresponding global minimum configuration, for this specific cluster size and composition. The knowledge of global and local minima is a preliminary step in the study of more complex theoretical and experimental analysis of sub-nanoparticles, such as those identified in this research. The construction of tree-type disconnectivity graphs facilitates an understanding of the possible structural interconversion between icosahedron-based geometrical isomers and other multitwinned conformations of the $Pd_{12}Pt_1$ cluster. Our results provide a full energetic description of these local minima structures, their place on the energy landscapes, as well as those configurations closely connected to the icosahedral global minimum structure. The energetics of the low-lying structures predicted by the Gupta potential are essentially confirmed through DFT computations, additionally finding that icosahedral and biplanar structures are also likely to coexist under the same physical conditions. Considering that the modeling of the interatomic interactions between the constituent atoms is a complex task, having realistic model potentials coupled with high-level theoretical calculations will facilitate the PES exploration of larger Pd–Pt bimetallic nanoparticles (also displaying different concentrations of Pd and Pt atoms); thus allowing the prediction of their corresponding ground-state configurations with a good degree of certainty. In this context, the combination of theoretical approaches and state-of-the-art computational tools become crucial in the development of novel tailor-made materials at the nanoscale, underpinning experimental studies. In view of the increasing relevance of sub-nanoparticles in technologically important processes such as heterogeneous catalysis, we expect that our theoretical results will stimulate the realization of experiments on systems such as the one studied here, with new techniques enabling finite temperature measurements to

be carried out on real systems, as well as other theoretical studies modeling free and supported binary nanoparticles.

Acknowledgements

RPC and MDF are grateful to CONACYT for the award of a PhD scholarship. APA acknowledges financial support from CONACYT through grants 24060 and 180424. RLJ is grateful for financial support from COST Action MP0903: ''Nanoalloys as Advanced Materials: From Structure to Properties and Applications''.

References

1 R. Ferrando, J. Jellinek and R. L. Johnston, *Chem. Rev.*, 2008, **108**, 845.
2 N. Sounderya and Y. Zhang, *Recent Pat. Biomed. Eng.*, 2008, **1**, 34.
3 O. V. J. Salata, *J. Nanobiotechnol.*, 2004, **2**, 3.
4 F. Baletto and R. Ferrando, *Rev. Mod. Phys.*, 2005, **77**, 371.
5 W. He, X. Wu, J. Liu, X. Hu, K. Zhang, S. Hou, W. Zhou and S. Xie, *Chem. Mater.*, 2010, **22**, 2988.
6 H.-J. Freund, *Surf. Sci.*, 2002, **500**, 271.
7 J. K. Nørskov, T. Bligaard, J. Rossmaisl and C. H. Christensen, *Nat. Chem.*, 2009, **1**, 37.
8 J. L. Renouprez, A. J. Rousset, A. M. Cadrot, Y. Y. Soldo and L. Stievano, *J. Alloys Compd.*, 2001, **328**, 50.
9 J. L. Rousset, L. Stievano, F. J. Cadete-Santos-Aires, C. Geantet, A. J. Renouprez and M. Pellarin, *J. Catal.*, 2001, **202**, 163.
10 D. Bazin, D. Guillaume, Ch. Pichon, D. Uzio and S. Lopez, *Oil Gas Sci. Technol.*, 2005, **60**, 801.
11 C. Burda, X. Chen, R. Narayanan and M. A. El-Sayed, *Chem. Rev.*, 2005, **105**, 1025.
12 S. E. Habas, H. Lee, V. Radmilovic, G. A. Somorjai and P. Yang, *Nat. Mater.*, 2007, **6**, 692.
13 L. D'Souza and S. Sampath, *Langmuir*, 2000, **16**, 8510.
14 S. I. Sanchez, M. W. Small, J. M. Zuo and R. G. Nuzzo, *J. Am. Chem. Soc.*, 2009, **131**, 8683.
15 R. S. Berry, *Chem. Rev.*, 1993, **2379**, 93.
16 D. J. Wales, *Energy Landscapes*, Cambridge University Press, Cambridge, England, 2003.
17 D. J. Wales and J. P. K. Doye, *J. Chem. Phys.*, 2003, **119**, 12409.
18 J. Jellinek and E. B. Krissinel, in *Theory of Atomic and Molecular Clusters*, ed. J. Jellinek, Springer-Verlag, Berlin, 1999, p. 277.
19 J. P. K. Doye and L. Meyer, *Phys. Rev. Lett.*, 2005, **95**, 063401.
20 J. C. Schön and M. Jansen, *Z. Krist.*, 2001, **216**, 307; J. C. Schön and M. Jansen, *Z. Krist.*, 2001, **216**, 361.
21 J. C. Schön and M. Jansen, *Int. J. Mater. Res.*, 2009, **100**, 135.
22 S. M. Woodley and R. Catlow, *Nat. Mater.*, 2008, **7**, 937.
23 J. C. Schön, K. Doll and M. Jansen, *Phys. Status Solidi B*, 2010, **247**, 23.
24 R. Ferrando, A. Fortunelli and R. L. Johnston, *Phys. Chem. Chem. Phys.*, 2008, **10**, 640.
25 S. E. Schönborn, S. Goedecker, S. Roy and A. R. Oganov, *J. Chem. Phys.*, 2009, **130**, 144108.
26 L. O. Paz-Borbón, T. V. Mortimer-Jones, R. L. Johnston, A. Posada-Amarillas, G. Barcaro and A. Fortunelli, *Phys. Chem. Chem. Phys.*, 2007, **9**, 5202.
27 F. Pittaway, L. O. Paz-Borbón, R. L. Johnston, H. Arslan, R. Ferrando, C. Mottet, G. Barcaro and A. Fortunelli, *J. Phys. Chem. C*, 2009, **113**, 9141.
28 J. P. K. Doye and D. J. Wales, *J. Phys. Chem. A*, 1997, **101**, 5111.
29 R. Gehrke and K. Reuter, *Phys. Rev. B*, 2009, **79**, 085412.
30 G. Barcaro and A. Fortunelli, *Phys. Rev. B*, 2007, **76**, 165412.
31 J. C. Schön, H. Putz and M. Jansen, *J. Phys.: Condens. Matter*, 1996, **8**, 143.
32 J. C. Schön, *Ber. Bunsen-Ges. Phys. Chem.*, 1996, **100**, 1388.
33 M. J. Goldstein, *J. Chem. Phys.*, 1969, **51**, 3728.
34 V. K. De Souza and D. Wales, *J. Chem. Phys.*, 2009, **130**, 194508.
35 J. C. Schön and M. Jansen, *Angew. Chem., Int. Ed. Engl.*, 1996, **35**, 1286.
36 H. Jónsson and H. C. Andersen, *Phys. Rev. Lett.*, 1988, **60**, 2295.
37 E. Urrutia-Bañuelos, A. Posada-Amarillas and I. L. Garzón, *Phys. Rev. B*, 2002, **66**, 144205.
38 K. H. Hoffmann and P. Sibani, *Phys. Rev. A*, 1988, **38**, 4261.
39 O. M. Becker and M. Karplus, *J. Chem. Phys.*, 1997, **106**, 1495.
40 A. Heuer, *Phys. Rev. Lett.*, 1997, **78**, 4051.
41 D. J. Wales, M. A. Miller and T. R. Walsh, *Nature*, 1998, **394**, 758.
42 P. Hohenberg and W. Kohn, *Phys. Rev.*, 1964, **136**, B864.
43 W. Kohn and L. S. Sham, *Phys. Rev.*, 1965, **140**, A1133.
44 V. Rossato, M. Guillope and B. Legrand, *Philos. Mag. A*, 1989, **59**, 321.
45 I. L. Garzón, K. Michaelian, M. R. Beltrán, A. Posada-Amarillas, P. Ordejón, E. Artacho, D. Sánchez-Portal and J. M. Soler, *Phys. Rev. Lett.*, 1998, **81**, 1600.
46 C. Massen, T. V. Mortimer-Jones and R. L. Johnston, *J. Chem. Soc., Dalton Trans.*, 2002, 4375.
47 B. Delley, *J. Chem. Phys.*, 1990, **92**, 508.
48 B. Delley, *J. Chem. Phys.*, 2000, **113**, 7756.
49 We have used DMol3, version 6.0.
50 J. P. Perdew, K. Burke and M. Ernzerhof, *Phys. Rev. Lett.*, 1996, **77**, 3865.
51 B. Delley, *Phys. Rev. B*, 2002, **66**, 155125.
52 C. G. Broyden, *IMA J. Appl. Math.*, 1970, **6**, 222.
53 R. Fletcher, *Comput. J.*, 1970, **13**, 317.
54 D. Goldfarb, *Math. Comput.*, 1970, **24**, 23.
55 D. F. Shanno, *Math. Comput.*, 1970, **24**, 647.
56 C. Roberts, R. L. Johnston and N. T. Wilson, *Theor. Chem. Acc.*, 2000, **104**, 123.
57 D. M. Deaven and K. M. Ho, *Phys. Rev. Lett.*, 1995, **75**, 288.
58 R. L. Johnston, *Dalton Trans.*, 2003, 4193.
59 D. J. Borbón-González, R. Pacheco-Contreras, A. Posada-Amarillas, J. C. Schön, R. L. Johnston and J. M. Montejano-Carrizalez, *J. Phys. Chem. C*, 2009, **113**, 15904.
60 C. Zhu, R. H. Byrd and J. Nocedal, *Assoc. Comput. Mach., Trans. Math. Software*, 1997, **23**, 550.
61 R. Pacheco-Contreras, M. Dessens-Félix, D. J. Borbón-González, L. O. Paz-Borbón, R. L. Johnston, J. C. Schön and A. Posada-Amarillas, *J. Phys. Chem. A*, 2012, **116**, 5235.
62 D. Faken and H. Jónsson, *Comput. Mater. Sci.*, 1994, **2**, 279.

63 J. C. Schön, M. A. C. Wevers and M. Jansen, *J. Phys.: Condens. Matter*, 2003, **15**, 5479.
64 J. D. Bernal, *Proc. R. Soc. London, Ser. A*, 1964, **280**, 299.
65 P. J. Steinhardt, D. R. Nelson and M. Ronchetti, *Phys. Rev. Lett.*, 1981, **47**, 1297.
66 C. Zheng, R. Hoffmann and D. R. Nelson, *J. Am. Chem. Soc.*, 1990, **112**, 3784.
67 G. Vázquez-Polo and M. José-Yacamán, *Mater. Res. Soc. Symp. Proc.*, 1990, **174**, 163.
68 J. J. Velázquez-Salazar, R. Esparza, S. J. Mejía-Rosales, R. Estrada-Salas, A. Ponce, F. L. Deepak, C. Castro-Guerrero and M. José-Yacamán, *ACS Nano*, 2011, **5**, 6272.
69 C. M. Chang and M. Y. Chou, *Phys. Rev. Lett.*, 2004, **93**, 133401.
70 J. Rogan, G. García, J. A. Valdivia, W. Orellana, A. H. Romero, R. Ramírez and M. Kiwi, *Phys. Rev. B*, 2005, **72**, 115421.
71 T. Futschek, J. Hafner and M. Marsman, *J. Phys.: Condens. Matter*, 2006, **18**, 9703.
72 F. Aguilera-Granja, M. B. Torres, A. Vega and L. C. Balbás, *J. Phys. Chem. A*, 2012, **116**, 9353.
73 C. H. Hu, C. Chizallet, C. Mager-Maury, M. Corral-Valero, P. Sautet, H. Toulhoat and P. Raybaud, *J. Catal.*, 2010, **274**, 99.
74 H. Elgavi, C. Krekeler, R. Berger and D. Avnir, *J. Phys. Chem. C*, 2012, **116**, 330.
75 R. Ferrando, A. Fortunelli and R. L. Johnston, *Phys. Chem. Chem. Phys.*, 2008, **10**, 640.